DEPARTMENT OF SCIENCE AND TECHNOLOGY,
ANTARCTIC DIVISION

AUSTRALIAN NATIONAL
ANTARCTIC RESEARCH EXPEDITIONS

A N A R E
S C I E N T I F I C
R E P O R T S

SERIES A(4) GLACIOLOGY

PUBLICATION NO. 128

A PRELIMINARY INVESTIGATION OF THE PHYSICAL CHARACTERISTICS OF THE VAHSEL GLACIER, HEARD ISLAND

I.F. ALLISON

AUSTRALIAN GOVERNMENT PUBLISHING SERVICE
CANBERRA 1980

ISBN 0 642 01687 9

Printed by the Commonwealth Government Printing Unit, Melbourne

CONTENTS

FIGURES

TABLES

A PRELIMINARY INVESTIGATION OF THE PHYSICAL CHARACTERISTICS OF THE VAHSEL GLACIER, HEARD ISLAND

By I. F. Allison

Antarctic Division, Department of Science and Technology, Melbourne, Australia.

ABSTRACT

During February 1971 preliminary measurements were made on the Vahsel Glacier, Heard Island, in the South Indian Ocean. Results are presented of the surface velocity, strain-rate, surface profile, gravimetric ice thickness and ablation rates along a line across the glacier 200 m above sea level (a.s.l.). From the measurements estimates are made of the mass balance and equilibrium state of the glacier.

Despite the appreciable errors associated with short term measurements the results give a useful indication of the present dynamics of the glacier.

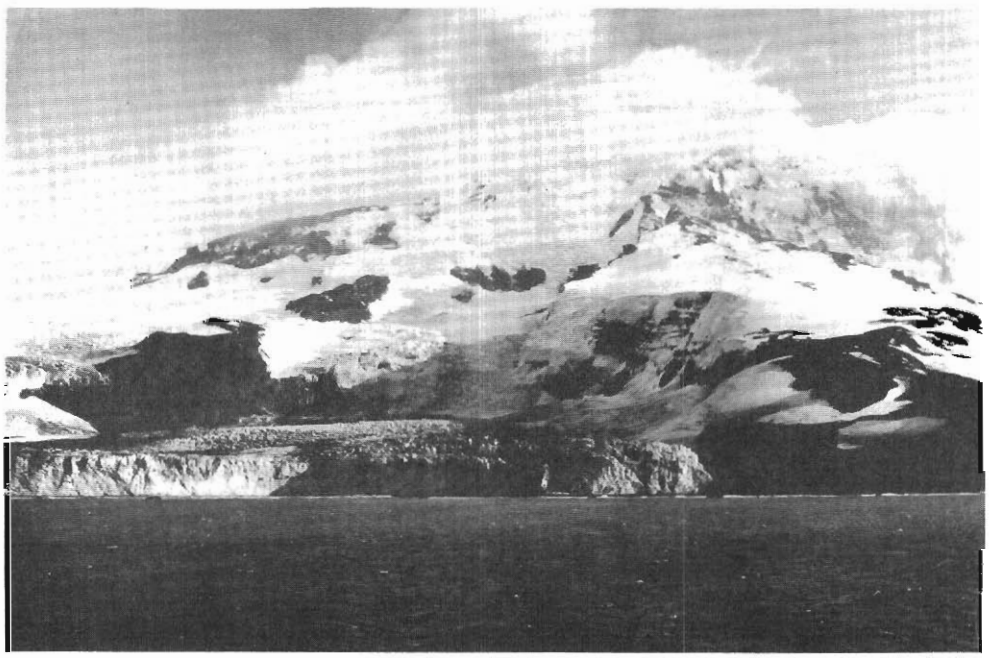

Plate 1. Heard Island from Corinthian Bay with glacier tongue in foreground. (Photograph by I. Dillon).

1. INTRODUCTION

Heard Island lies south of the Antarctic convergence in the Southern Indian Ocean at 73°30'E longitude and 53°05'S latitude. The island is about 44 km long and 19 km broad and is dominated by the large dome of Big Ben, the highest point of which is the active volcano Mawson Peak (2745 m) (Fig. 1.1). Big Ben is of volcanic origin, being built up of tuffs and lava flows.

The island is heavily glaciated with over 80 per cent of the area being covered with ice. Numerous glaciers flow from the rim of Big Ben, down steep chutes wnere they are heavily broken with large crevasses and seracs, and level out as they reach the coast. Many of the glaciers end at the sea in ice cliffs up to 50 m high but none are actually afloat. There is evidence of considerable ablation at the ice cliffs by the action of the sea but only relatively small pieces of ice are broken off. The glaciers show poor separation from their neighbours and most have badly broken surfaces.

A small ice cap and several small glaciers are also present on the Laurens Peninsula, to the north west of the main mass of the island.

1.1 Previous Glaciological Studies

From 1947 to 1955 a base at Atlas Cove was continuously occupied by the Australian National Antarctic Research Expeditions (A.N.A.R.E.) and short visits to the island were made in 1963, 1965 and 1969.

Observations on the movement of the glacier fronts (Budd (1964), Budd (1970), Budd and Stephenson (1970)) showed slight recession of some glaciers by 1947 becoming widespread by 1954. Major recession of all glaciers was noted in 1963, but by 1965 a readvance of some glaciers had commenced. In 1969 the glaciers of Corinthian Bay had readvanced to the 1954 position.

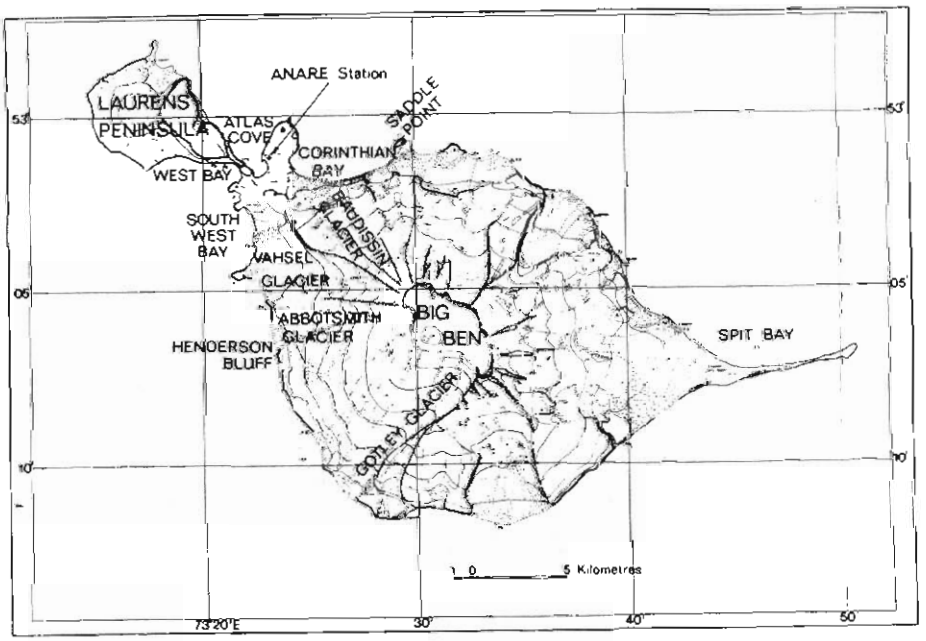

Figure 1.1 Heard Island.

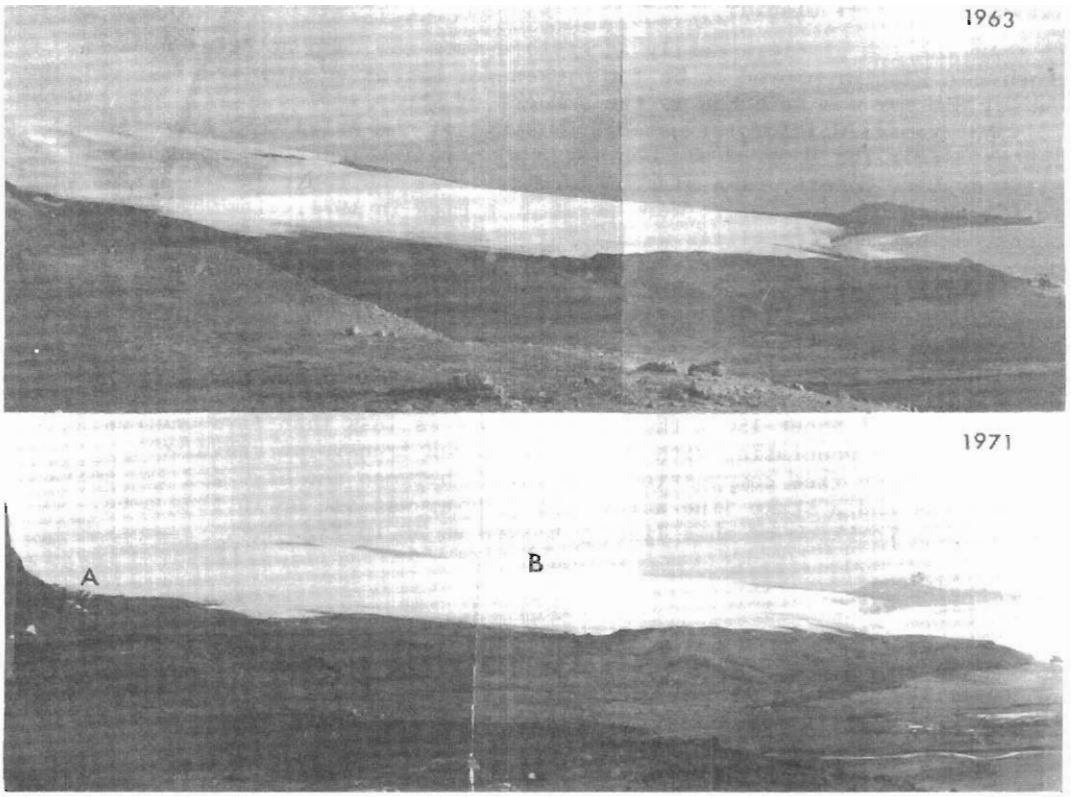

Figure 1.2 Lower Vahsel Glacier from Mt. Drygalski. Stake line between A and B.

The only recorded previous physical measurements on the Heard Island glaciers are those reported by Lambeth (1950). Velocities measured in 1948 at the centre of the Baudissin Glacier, at an elevation of about 90 m a.s.l., indicated an average movement rate of approximately 110 m a^{-1} for the period 11 September to 20 October, and a mean movement of approximately 330 m a^{-1} between 20 October and 8 December. Ablation measurements on the same glacier at an altitude of about 40 m a.s.l. showed an ablation of about 0.35 m for the month of November.

1.2 1971 Expedition to Heard Island

A French expedition visited Heard Island during the austral summer of 1971 to conduct a programme of research on coupled magnetic phenomena, and the administration of Terres Australes et Antarctiques Francaises invited Australian participation in the expedition. The final complement of the party was fourteen men, five being Australians. The participation of an Australian contingent in the expedition allowed a glaciologist to be included in the party, with the aim of commencing detailed measurements on the glaciers close to the base camps.

The expedition party was landed on Heard Island from the M.V. *Gallieni* on January 25, and was evacuated on March 10. During the six week stay on the island the bulk of the party resided at the old A.N.A.R.E. station at Atlas Cove.

1.3 The Vahsel Glacier

Of the two glaciers easily accessible from the camp at Atlas Cove the Baudissin Glacier proved to be too broken for extensive work and instead the Vahsel Glacier was selected as the subject of study.

The Vahsel Glacier, situated 5 km south of the Atlas Cove camp, flows westward from The Dome of Big Ben (2408 m). In its lower reaches the flow is split by Cape Gazert. The glacier terminates at the coast in ice cliffs which to the north of Cape Gazert were about 16 m high in 1971. Lambeth (1950) reported that the ice cliffs were about 40 m high in 1948. In 1963, photographs show a height of approximately 10 m. Fig. 1.2 shows the lower part of the Vahsel Glacier photographed from Mt. Drygalski (Fig. 2.1). Comparison of the 1963 and 1971 photographs shows considerable advance of the glacier front since 1963.

The upper part of the glacier is badly broken with many heavily seraced domes and a surface slope of greater than 30° at the highest levels. Below an elevation of about 150 m the surface slope is less than five degrees and the surface is undulating with regularly spaced transverse crevasses.

A crevasse free compression zone exists between the high and low surface slope areas and a stake line across the glacier was set up in this area. The approximate position of this line is marked as AB in Fig. 1.2.

2. ABLATION

A line of nine stakes was set up across the Vahsel Glacier at an elevation of about 150 to 200 m on 4 February 1971. An additional two stakes were placed in a line in the direction of flow near the centre of the glacier. The length of the main line was 2280 m and the position of the stakes is shown in Figure 2.1. The stakes used were one inch diameter, white painted canes, sunk to a depth of one metre in the ice. The line of stakes did not extend right to the rock at the southern edge of the glacier because of the highly crevassed surface in this region.

The surface in the region of the stake line during February was typical of a melting glacier. Melt streams and puddles were prevalent at the beginning of the month but decreased in number with time; little surface water was evident after the last week in February. A permanent snow cover started to form (especially in the higher areas) after the end of February and 70 mm of new snow was measured at stake G14 on 5 March. The ice at either edge of the glacier was noticeably dirtier than that in the centre due to the presence of dust particles. An obvious snow line existed about 50 m higher than the stake line and the presence of this, at the end of the major ablation period, can be taken as an indication of the position of the firn line at about 250 m a.s.l.

Measurements of the surface height on the stakes were made several times during February and early March and the results of these ablation measurements are shown in Table 2.1 (page 6). The mean ablation rate of all stakes during a 24 day period in February was 24 mm of ice per day. From a comparison of mean monthly ablation values expressed as percentages of the annual ablation for northern hemisphere glaciers (Mellor, 1964), the ablation during February on the Vahsel might be expected to be about 20 per cent of the annual ablation. Hence the annual ablation would be of the order of three to four metres of ice. Estimates of the annual precipitation are discussed in Section 8.

Although the data of Table 2.1 indicates a slight tendency for the ablation to decrease with the elevation (as determined in Section 5) this

The following mountain stations were used as the fixed stations for the resections:

1	-	Cape Gazert	2	-	Mt. Andrée
3	-	Mt. Aubert de la Rue	4	-	Mt. Drygalski
5	-	un-named peak (220 m) SE of Mt. Drygalski; unofficially named Mt. Schmidt			

Obviously the strength of the resections will increase as the observed angle between the fixed stations increases. However, Cape Gazert was only interdivisible from stakes G15, G14 and G05 and the more northerly stakes could only be weakly resected using Mt. Andrée, Aubert de la Rue, Drygalski and Schmidt (2, 3, 4, 5).

On misty occasions Mt. Andrée became invisible against the bulk of the Laurens Peninsula (normally in cloud) and only the extremely weak resection to Aubert de la Rue, Drygalski and Schmidt (3, 4, 5) could be obtained.

Horizontal angles between stakes, and the distance between them (either from stadia measurements during levelling, or from chaining) were used as a check on the resected positions. The positioning of weakly resected stakes was improved by including traverse data from a more strongly fixed one. The position of stakes G43 and G10 was determined with respect to G11 from the chaining data.

3.1 Errors of velocity determination

Errors in stake positioning from resection arise due to two causes:

(a) Errors in measured angles

This becomes increasingly important as the magnitude of the observed angle decreases. The resection data was solved to yield the distance (R) and bearing (ε) from Mt. Drygalski to the stake and the errors in R (δR) and

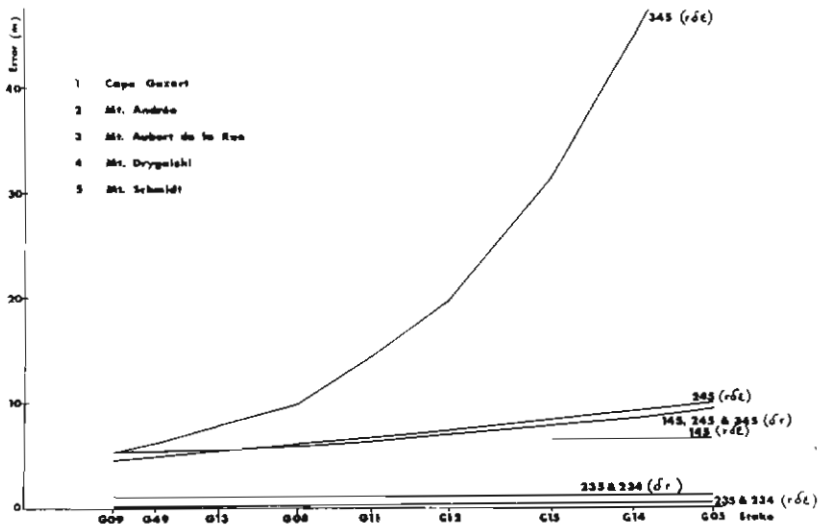

Figure 3.1 Errors in positioning by resection due to a 10" error in angle measurement.

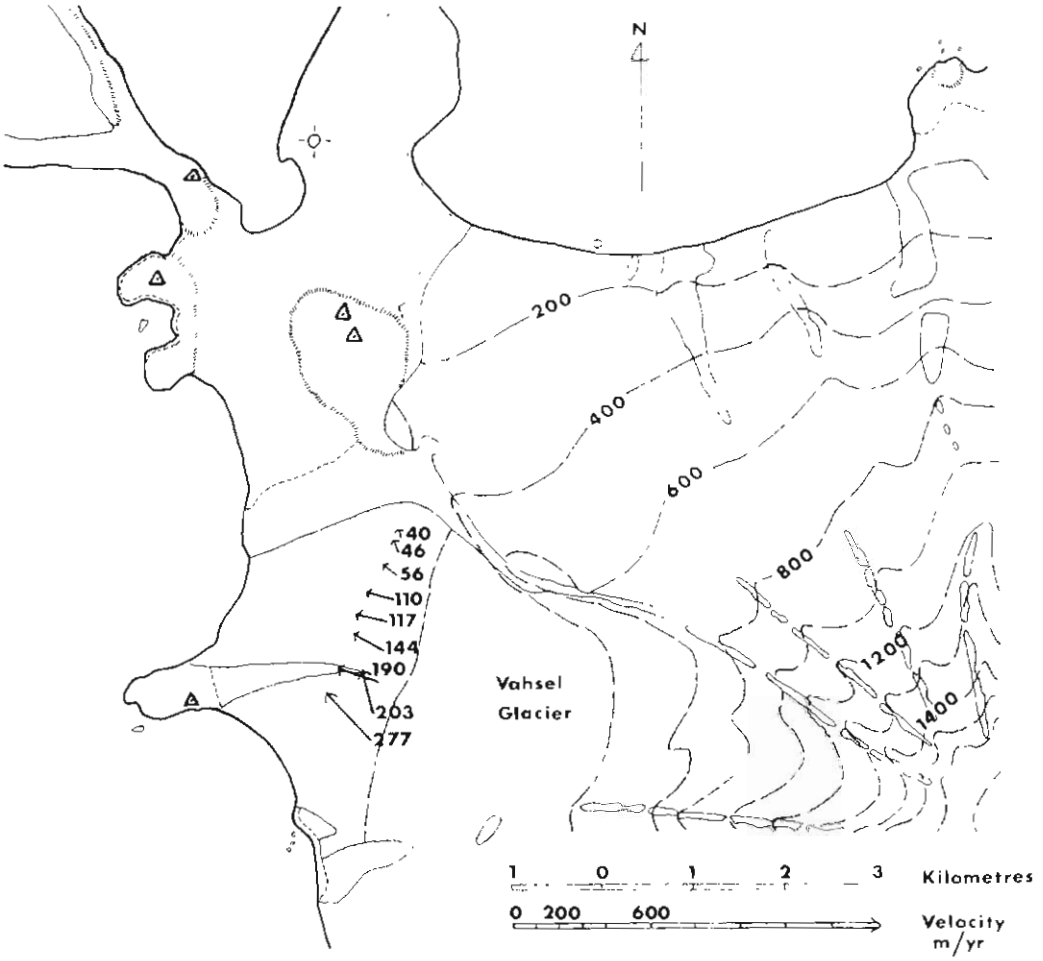

Figure 3.2 Velocity vectors on the Vahsel Glacier.

in arc length (Rδε) resulting from an observed angle error of ten seconds of arc are plotted in Figure 3.1 for different stakes and resections. Obviously resections including Mounts Drygalski and Schmidt (4 and 5) are the weakest.

The data of Figure 3.1 was used to define error areas for the final and initial stake positions. In some cases the error with resection alone is considerably larger than the observed movement, but the final error has been reduced by including the traverse data. The limits of the magnitude and the directions of movement possible with the calculated position errors are quoted in Table 3.1.

(b) Errors in position of the mountain stations

This will lead to significant error in the position of the stakes because, with the exception of Mount Drygalski, the mountain triangulation stations could not be easily identified from the glacier. A computer program was run to determine the positions of the mountain stations which were compatible with the least squares best fit of the stakes from different resections and the traverse data. The computed mountain positions were identified, in one plane,

Stake	Initial position of stake. Local Transverse Mercator co-ordinates (metre) with respect to Mt. Drygalski.		Movement of stake (metre)	Number of days between measurements	Ice Velocity	
	Easting	Northing			Magnitude m a^{-1}	Direction (true)
G09	627	-2531	2.3 ±1.8	21	40 ±32	351^{o} $\pm40^{o}$
G49	604	-2690	2.9 ±1.2	23	46 ±19	342^{o} $\pm13^{o}$
G13	570	-2926	3.2 ±1.8	21	56 ±32	311^{o} $\pm40^{o}$
G08	525	-3213	8.1 ±4.9	27	110 ±66	286^{o} $\pm45^{o}$
G11	484	-3495	9.3 ±3.0	29	117 ±38	288^{o} $\pm36^{o}$
G12	439	-3781	9.1 ±3.0	23	144 ±48	302^{o} $\pm27^{o}$
G15	378	-4163	10.9 ±1.8	21	190 ±32	293^{o} $\pm11^{o}$
G14	324	-4464	11.7 ±2.1	21	203 ±37	345^{o} $\pm20^{o}$
G05	283	-4765	16.0 ±5.2	21	277 ±90	318^{o} $\pm21^{o}$
G43	732	-3544	12.3 ±3.0	29	155 ±38	306^{o} $\pm36^{o}$
G10	269	-3453	9.8 ±3.0	29	123 ±38	292^{o} $\pm36^{o}$

Table 3.1 Ice movement data

on photo theodolite photographs taken from Mount Drygalski, and, although differing from established survey triangulation stations, they compared well with the resection stations as identified from field book sketches.

Errors in the relative positions of the stakes due to errors in the mountain positions will be small (and have not been included in the velocity errors), as all stakes were resected from the stations on the mountains during both the initial and final surveys. However, the absolute position of the line may be in error by as much as 100 m in any direction.

3.2 Velocity

The computed ice velocities and associated errors are listed in Table 3.1 and the velocity vectors are shown in Figure 3.2. In all cases these velocities appear reasonable. The strong northward component of velocity at stakes G09, G49 and G14 can be explained by the north-south slope of the ice surface in these areas.

4. STRAIN-RATES AT G11

The three central stakes of the transverse line and the two extra stakes along the direction of flow were used as a strain grid centred on stake G11. The radial distances from G11 to the outer stakes of the grid were chained and the horizontal angles between stakes read at G11. The length of the radial arms was about 250 m. Chaining was done with a 100 m steel tape, hung in catenary,

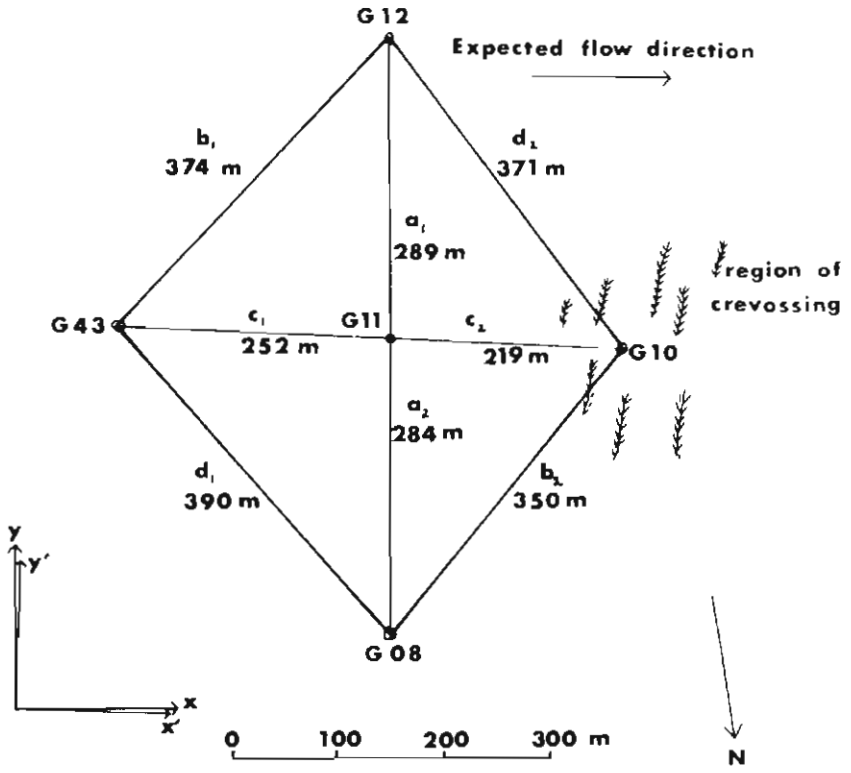

Figure 4.1 Layout of strain grid at G11.

ORIENTATION OF GRID ARMS RELATIVE TO AXES 0_x, 0_z

a_1	0^o		b_1	42^o	c_1	93^o	d_1	140^o
a_2	0^o		b_2	39^o	c_2	93^o	d_2	143^o
mean:	0^o			40.5^o		93^o		142.5^o

Orientation relative to $0'_x$, $0'_z$ (rotated 1.5^o clockwise from 0_x, 0_z)

-1.5^o 39^o 91.5^o 141^o

Strain-rate	$\dot{\varepsilon}_0$ a	$\dot{\varepsilon}_{45}$ b	$\dot{\varepsilon}_{90}$ c	$\dot{\varepsilon}_{135}$ d	$\dot{\varepsilon}_0 + \dot{\varepsilon}_{90}$	$\dot{\varepsilon}_{45} + \dot{\varepsilon}_{135}$	$(\dot{\varepsilon}_0+\dot{\varepsilon}_{90})-(\dot{\varepsilon}_{45}+\dot{\varepsilon}_{135})$	
1	-0.010	+0.037	-0.002	-0.079				
2	-0.005	-0.021	-0.064	-0.008				
Mean	-0.008	+0.008	-0.033	-0.043	-0.041	-0.036	-0.005	

$\dot{\varepsilon}_x$ = -0.032	$\dot{\varepsilon}_{yx}$ = +0.026	$\dot{\varepsilon}_y$ = -0.006	Standard error = ±0.002

Principal Strain-Rates:

$\dot{\varepsilon}_1$ = -0.048	$\dot{\varepsilon}_2$ = +0.038	$\dot{\varepsilon}_3$ = +0.010	ϕ = angle between $0'_y$ and $\dot{\varepsilon}_3$ = -31.5^o

Table 4.1 Strain-rates at stake G11 (all strain-rates in a^{-1})

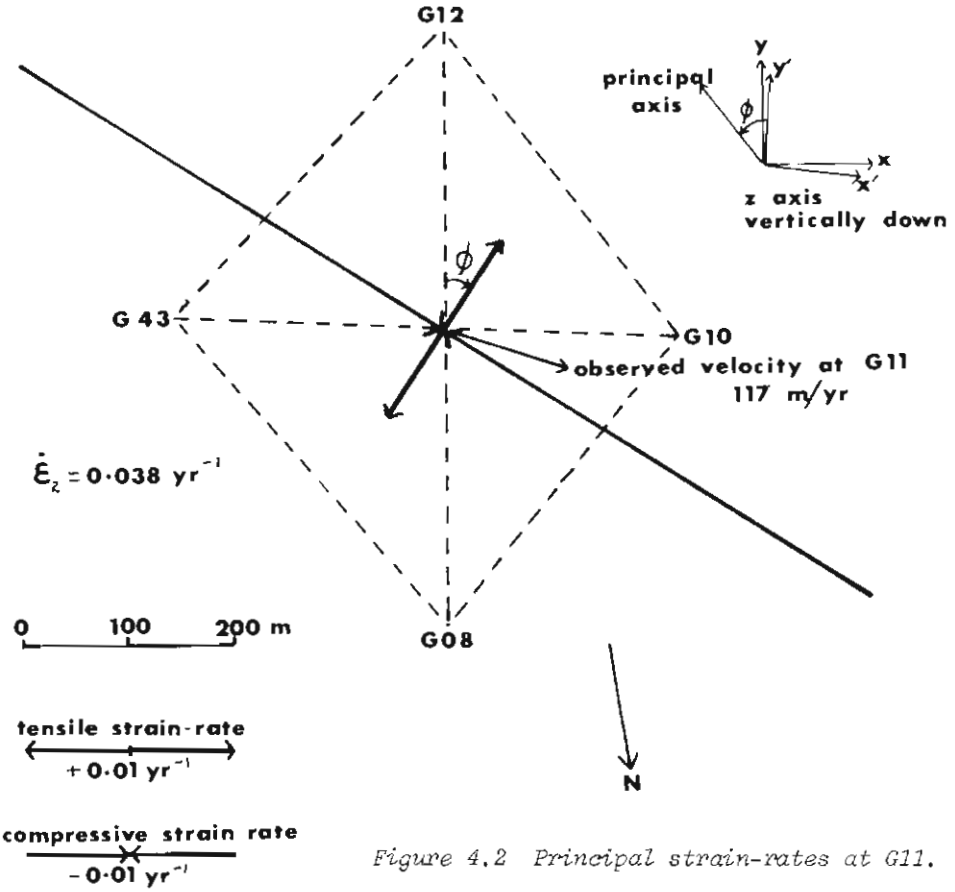

Figure 4.2 Principal strain-rates at G11.

and appropriate corrections were made for slope, sag and chain temperature. The grid was surveyed on both 4 February and 5 March 1971.

The layout of the strain grid is shown in Figure 4.1. Arms a_1, a_2, c_1 and c_2 were chained directly, whilst b_1, b_2, d_1 and d_2 were calculated from the measured angles and distance.

The strain-rates have been calculated by the method of Nye (1959) and are shown in Table 4.1. The strain-rate is defined by:

$$\dot{\varepsilon} = \frac{1}{\Delta t} \ell n \frac{L_f}{L_i}$$

where L_i and L_f are the initial and final lengths of the stake interval over the time interval Δt (= 29 days). Because the strain grid as laid out was not a perfect square it has been necessary to rotate the strain axes (0_x, 0_y) by 1.5 degrees to minimize the misalignment of the stakes with the strain directions of 0^o, 45^o, 90^o and 135^o. Even so the maximum misalignment with the new axes ($0_{x'}$, $0_{y'}$) is still 6^o.

Each of the strain-rates at G11 has been calculated from the mean of the strain in two "parallel" arms (e.g. $\dot{\varepsilon}_{45}$ from b_1 and b_2). That is, the strains calculated are the means at G11 over the area of the grid. Theoretically:

$$\dot{\varepsilon}_{45} + \dot{\varepsilon}_{135} = \dot{\varepsilon}_0 + \dot{\varepsilon}_{90}$$

and the actual deviation from this is found to be 0.005 yr^{-1}.

The three strain-rate components $\dot{\varepsilon}_x$, $\dot{\varepsilon}_y$ and $\dot{\varepsilon}_{yx}$ have been found from $\dot{\varepsilon}_0$, $\dot{\varepsilon}_{45}$, $\dot{\varepsilon}_{90}$, and $\dot{\varepsilon}_{135}$ by the least squares solution:

$$\dot{\varepsilon}_x = -1/4\ \dot{\varepsilon}_0 + 1/4\ \dot{\varepsilon}_{45} + 3/4\ \dot{\varepsilon}_{90} + 1/4\ \dot{\varepsilon}_{135}$$

$$\dot{\varepsilon}_{yx} = 1/2\ \dot{\varepsilon}_{45} - 1/2\ \dot{\varepsilon}_{135}$$

$$\dot{\varepsilon}_y = 3/4\ \dot{\varepsilon}_0 + 1/4\ \dot{\varepsilon}_{45} - 1/4\ \dot{\varepsilon}_{90} + 1/4\ \dot{\varepsilon}_{135}$$

and the standard error in $\dot{\varepsilon}_x$ and $\dot{\varepsilon}_y$ is $\sqrt{3}|v|$ and in $\dot{\varepsilon}_{yx}$ is $\sqrt{2}|v|$ where $|v|$ is the residual of the four measured values.

The values of principal strain-rate have been derived assuming that the principal strain axes are parallel to the principal shear stress, that the upper surface of the ice is free of shear stress, and that the ice is incompressible.

i.e. $$\dot{\varepsilon}_{xz} = \dot{\varepsilon}_{zy} = 0$$

and $$\dot{\varepsilon}_2 = \dot{\varepsilon}_z = -(\dot{\varepsilon}_x + \dot{\varepsilon}_y)$$

Then the principal strain-rates in the x-y plane are given by:

$$\dot{\varepsilon}_1 = 1/2\ (\dot{\varepsilon}_x + \dot{\varepsilon}_y) - \sqrt{[1/4(\dot{\varepsilon}_x - \dot{\varepsilon}_y)^2 + \dot{\varepsilon}_{yx}^2]}$$

$$\dot{\varepsilon}_2 = 1/2\ (\dot{\varepsilon}_x + \dot{\varepsilon}_y) + \sqrt{[1/4(\dot{\varepsilon}_x - \dot{\varepsilon}_y)^2 + \dot{\varepsilon}_{yx}^2]}$$

and $$\tan 2\phi = \frac{2\,\dot{\varepsilon}_{yx}}{\dot{\varepsilon}_x - \dot{\varepsilon}_y}, \quad -\pi/4 < \phi < \pi/4$$

where ϕ is the angle between 0_y, and the nearest principal axes (sense shown in Figure 4.2).

The calculated values of principal strain-rate are listed in Table 4.1 and the strain-rates are shown diagrammatically in Figure 4.2.

5. SURFACE PROFILES AND ELEVATIONS

The surface profile across the glacier was determined by optical levelling along the stake line. Total closure error of the levelling was less than 0.1 m. Surface profiles from the measured levels and from the stadia distances are plotted in Figures 6.6 and 6.7 (pages 22-23).

Vertical angles to Mount Drygalski were read at each stake and used to compute the elevation above sea level at that point. Using the level data, all elevations were reduced to give the elevation at G11. The final elevation at G11 was taken as the mean of all estimates (standard deviation of 0.2 m), and the elevation of the other stakes determined from this. It should be noted that, although the height difference between stakes has an error of less than 0.1 m, the absolute elevation above sea level may be in error by as much as ±1.5 m because of the uncertainty in the position of the line.

5.1 Change in elevation with time

A repeat optical levelling of the stake line was carried out 24 days after the initial survey to determine the change in level of the ice surface. Change of level at any stake moving down the glacier ($\partial h/\partial t$), is due to the

Stake	Height above sea level (m) 28/2/71	Stadia distance from GM (m)	Elevation above GM (m) 4/2/71	28/2/71	$\frac{\partial h}{\partial t}$ m/day	Accumulation/ Ablation A m/day	$(A - \frac{\partial h}{\partial t})$ m/day	m/a	error m/a	α degrees of arc	Vtanα m/a	error m/a	Divergence term (for period 4/2 to 28/2) m/a	error m/a
G09	129.7	32	4.36	4.13	-0.010	-0.032	-0.022	-8.1	±3.0	7	4.9	±5.3	-13.0	±8.3
G49	145.6	189	20.34	20.03	-0.013	-0.025	-0.012	-4.3	±3.0	4	3.2	±2.9	- 7.5	±5.9
G13	152.3	429	27.11	26.72	-0.016	-0.025	-0.009	-3.1	±3.0	1.5	1.5	±1.8	- 4.6	±4.8
G08	153.0	718	27.92	27.38	-0.023	-0.023	-0.000	-0.0	±3.0	1.5	2.9	±3.7	- 2.9	±6.7
G11	164.1	1002	39.29	38.54	-0.031	-0.022	+0.009	+3.4	±3.0	1.4	2.8	±0.9	+ 0.6	±3.9
G12	167.7	1291	42.99	42.17	-0.034	-0.027	+0.007	+2.6	±3.0	1.5	3.8	±3.8	- 1.2	±6.8
G15	171.2	1678	47.01	45.65	-0.057	-0.019	+0.037	+13.6	±3.0	1.5	5.0	±4.2	+ 8.6	±7.2
G14	192.2	1981	69.10	66.65	-0.102	-0.025	+0.077	+28.3	±3.0	5	17.8	±10.3	+10.5	±13.3
G05	208.0	2282	83.68	82.41	-0.053	-0.026	+0.027	+ 9.9	±3.0	3	14.5	±12.0	- 4.6	±15.0
		Stadia distance from G11 (m)												
G43	183.6	265	59.35	58.05	-0.054	-0.021	+0.034	+12.3	±3.0	6.1	13.1	±4.0	- 0.8	±7.0
G10	159.7	220	34.61	34.13	-0.020	-0.023	-0.003	- 0.9	±3.0	1.3	3.5	±0.9	- 4.4	±3.9

Table 5.1 Elevation and levelling data

vertical component of ice movement, the net balance (A), and a flow divergence term, and can be expressed as:

$$\partial h/\partial t = A - V \tan \alpha - \frac{1}{\bar{Y}} \frac{\partial(\bar{Y}\bar{V}Z)}{\partial x}$$

where the glacier width $\bar{Y}$ and the velocity $\bar{V}$ are the means over a vertical column of ice. Z is the ice thickness, and α is the surface slope in the direction of ice movement. The elevation and levelling data is presented in Table 5.1.

The surface slope was measured at G43, G11 and G10 but has only been estimated at all other stakes and may be in error by as much as 2^{0}.

The divergence term $\frac{1}{\bar{Y}} \frac{\partial(\bar{Y}\bar{V}Z)}{\partial x}$ has been estimated from the above equation, but the very large errors effectively mask any significance of the estimate. The change in level of the ice surface is discussed further, in the context of the glacier equilibrium, in Section 8.

6. GRAVITY MEASUREMENTS AND ICE THICKNESS

The use of gravity measurements to determine ice thickness of valley glaciers is well known [e.g. Bull and Hardy(1956), Theil et al.(1957), Kanasewhich (1963), Corbato(1965), Crossley and Clarke(1970)]. Although the gravity anomalies cannot provide a unique solution for the bedrock depth, the method offers a quick and simple means of estimating ice thickness and glacier shape, especially on glaciers with difficult access.

A gravity survey across the Vahsel stake line was made on 28 February using a Worden gravimeter (W260A) with a dial constant of 0.1088 mgal per scale division (1 mgal = 10^{-5} m sec^{-2}). The gravity survey was made simultaneously with the repeat optical levelling of the ice surface. A total of 20 gravity stations, with an approximate spacing of 200 m, were established at the levelling change points.

To correct for meter drift and earth tide, several stations were reoccupied at regular intervals. The resultant drift curves are shown in Figure 6.1. The total drift has a mean of about 0.04 mgal per hour, and at no time exceeded 0.07 mgal per hour.

Repeatability of the reading, after drift corrections, was better than 0.1 mgal.

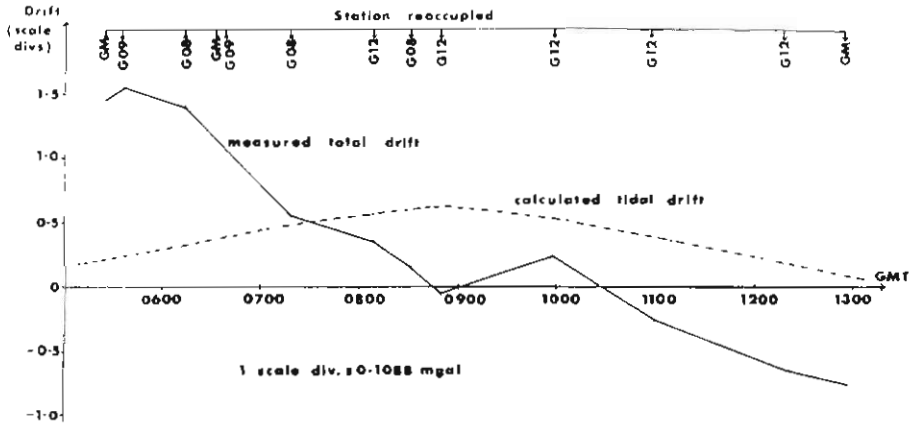

Figure 6.1 Drift of Worden gravimeter W260A on 28 February 1971.

6.1 Reduction of readings

The gravity readings are not tied to any absolute measurement and are expressed as the difference from the value at station GM. The following corrections were applied to the raw gravity data:

(a) Free air correction: This corrects for the variation of the force of gravity with the distance between the point of observation and the centre of mass of the Earth. The readings have been reduced to a datum line at the elevation of station GM by a correction of 0.3086h mgal, where h is the elevation difference between the observation station and GM. Elevation differences are known from the optical levelling to an accuracy of 0.1 m.

(b) Bouguer corrections: This corrects for an infinite slab of material between the observation point and datum level. The Bouguer correction is -41.85×10^{-6} hρ mgal, where ρ is the density of the intervening material. As all observation stations are above the level of GM, ρ has been taken as the density of ice (0.9×10^{3} kg m^{-3}), and the Bouguer corrections as - 0.0377h mgal. The error of the Bouguer and free air corrections combined is less than 0.03 mgal.

(c) Terrain correction: The intervening material between the observation point and the datum level is not an infinite slab as assumed in the

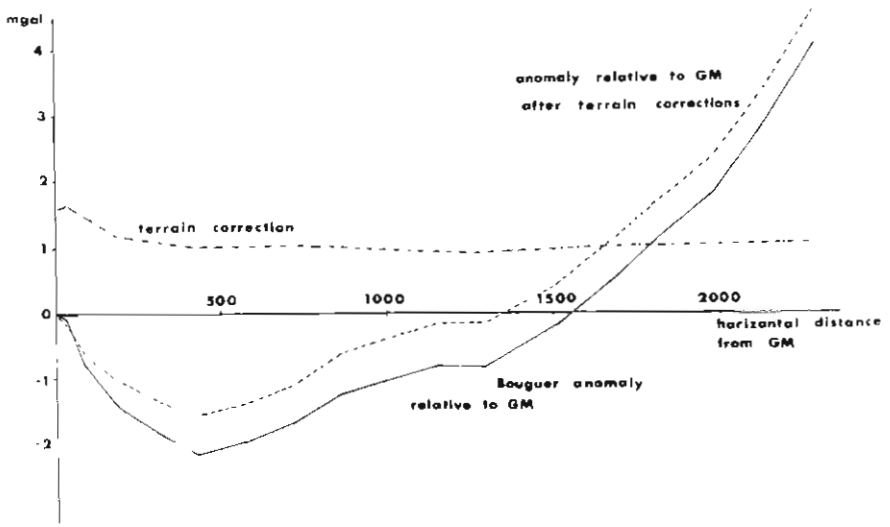

Figure 6.2 Gravity anomalies along transverse line.

Bouguer correction, and the terrain correction allows for varying surface altitudes around the observation point. The gravitational effect of the surrounding terrain at each station was estimated by using the graticule method of Hammer (1939).

In a mountainous area such as Heard Island, the terrain correction requires not only detailed information on the surrounding topography, but also a knowledge of the distribution of density variations in the area.

Not only is the available topographic map of Heard Island inaccurate, but also density variations are unknown because of the heavily glaciated nature of the island. Terrain corrections have been estimated for Hammer zones A to E (53.3 m to 390.1 m from the observation point) using a density

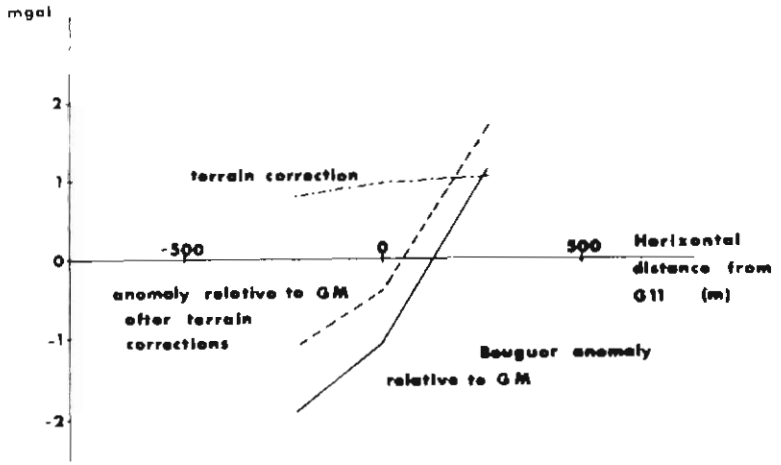

Figure 6.3 Gravity anomalies along longitudinal line.

of 2.2 x 10^3 kg m^{-3} (taken as a reasonable mean density for the distribution of ice and rock in these zones).

No estimate of the terrain correction for areas beyond Hammer zone 1 has been made as there is little information of ocean soundings around the island. However, if only the differences in terrain correction between the observation station and station GM are considered, then the contribution of the areas beyond Zone I should be small compared to closer zones.

Repeated computation of the terrain corrections showed a repeatability of about 0.2 mgal.

The magnitude of the terrain corrections is as high as 1.6 mgal, and the main variation of the correction along the line is due to the proximity of the northern-most stations to the sharp ridge between Big Ben and Mt. Drygalski.

(d) Regional gravity field: No data was available on regional variations and no correction was applied.

All corrections applied and the residual anomalies are listed in Tables 6.1 and 6.2 (pages 18-19), and are shown in Figures 6.2 and 6.3. Accuracy of the residual anomaly is ±0.5 mgal.

6.2 Interpretation

Consider the gravity value at P in the two situations depicted in Figure 6.4. In (i) the volume A, above the datum line, has been accounted for by the

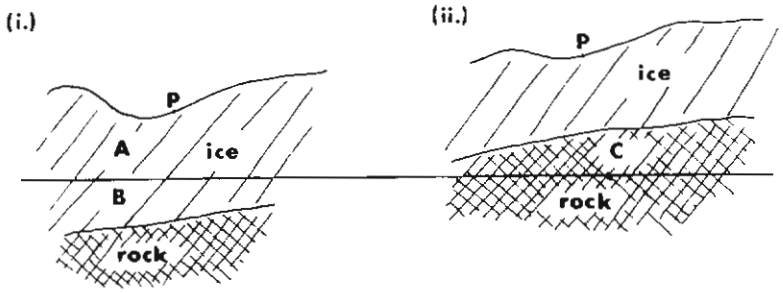

Figure 6.4 Residual anomaly detail.

Station	Horiz-ontal distance from GM (m)	Elevat-ion (m) 28/2/71	Elevat-ion relative to station GM h (m)	Differ-ence from gravity reading at GM (mgal)	Error in gravity differ-ences (± mgal)	Free air correct-ion +0.3086h (mgal)	Bouguer correct-ion -0.0377h (mgal)	Bouguer anomaly relative to GM (mgal)	Terrain correct-ion (mgal)	Terrain correct-ion relative to GM (mgal)	Resid-ual anomaly relative to station GM (mgal)
GM	0	125.6	0.00	0.00	0.00	+ 0.00	0.00	0.00	+1.60	0.00	0.00
G09	32	129.7	4.13	-1.24	0.09	+ 1.27	-0.16	-0.12	+1.65	+0.05	-0.07
*09	91	136.9	11.29	-3.67	0.09	+ 3.48	-0.43	-0.61		-0.19	-0.80
G49	189	145.6	20.03	-6.43	0.10	+ 6.18	-0.75	-1.00	+1.18	-0.42	-1.42
*49	326	150.7	25.12	-8.16	0.10	+ 7.75	-0.95	-1.36		-0.50	-1.86
G13	429	152.3	26.72	-8.79	0.09	+ 8.25	-1.01	-1.55	+1.01	-0.59	-2.14
*13	570	153.0	27.47	-8.82	0.09	+ 8.48	-1.04	-1.38		-0.58	-1.96
G08	718	153.0	27.38	-8.51	0.10	+ 8.45	-1.03	-1.09	+1.03	-0.57	-1.66
*08	862	158.2	32.61	-9.47	0.11	+10.06	-1.23	-0.63		-0.60	-1.23
G11	1002	164.1	38.54	-10.83	0.09	+11.89	-1.45	-0.39	+0.97	-0.63	-1.02
*11	1159	165.0	39.41	-10.83	0.09	+12.16	-1.49	-0.15		-0.65	-0.80
G12	1291	167.7	42.17	-11.57	0.09	+13.01	-1.59	-0.15	+0.93	-0.67	-0.82
*12	1520	167.1	41.54	-10.78	0.09	+12.82	-1.57	+0.47		-0.63	-0.16
G15	1678	171.2	45.65	-11.29	0.09	+14.09	-1.72	+1.08	+1.01	-0.59	+0.49
*15	1814	178.8	53.24	-12.73	0.09	+16.43	-2.01	+1.70		-0.58	+1.12
G14	1981	192.2	66.65	-15.69	0.09	+20.57	-2.51	+2.37	+1.04	-0.56	+1.81
*14	2141	201.7	76.15	-17.30	0.09	+23.50	-2.87	+3.33		-0.55	+2.78
G05	2282	208.0	82.41	-17.72	0.09	+25.43	-3.11	+4.61	+1.07	-0.53	+4.08

Table 6.1 Transverse profile - gravity readings, corrections and residual anomalies

Station	Horizontal distance from GII (m)	Elevation (m)	Elevation relative to station GM h (m)	Difference from gravity reading at GM (mgal)	Error in gravity differences (± mgal)	Free air correction +0.3086h (mgal)	Bouguer correction -0.0377h (mgal)	Bouguer anomaly relative to GM (mgal)	Terrain correction (mgal)	Terrain correction relative to GM (mgal)	Residual anomaly relative to station GM (mgal)
G43	+265	183.6	58.05	-14.04	0.09	+17.91	-2.19	+1.69	+1.02	-0.58	+1.11
G11	0	164.1	38.54	-10.83	0.09	+11.89	-1.45	-0.39	+0.97	-0.63	-1.02
G10	-220	159.7	34.13	-10.34	0.09	+10.53	-1.29	-1.09	+0.80	-0.80	-1.89

Table 6.2 Longitudinal profile - gravity readings, corrections and residual anomalies

Station	WITHOUT TERRAIN CORRECTION				INCLUDING TERRAIN CORRECTION			
	Observed Bouguer Anomaly (mgal)	Ice depth from datum (assuming ∞ Bouguer slabs) (m)	Final estimate of ice depth from datum Z (m)	Observed Bouguer anomaly - (Bouguer anomaly calculated for depth Z) (mgal)	Observed Bouguer Anomaly (mgal)	Ice depth from datum (assuming ∞ Bouguer slabs (m)	Final estimate of ice depth from datum Z (m)	Observed Bouguer anomaly - (Bouguer anomaly calculated for depth Z) (mgal)
GM	0.00	-20+	-20+	0.00	0.00	-20+	-20+	0.00
G09	-0.12	-21	-22	+0.03	-0.07	-21	-17	0.00
*09	-0.61	-28	-31	0.00	-0.80	-31	-33	0.00
G49	-1.00	-33	-36	+0.03	-1.42	-39	-42	0.00
*49	-1.36	-38	-40	+0.01	-1.86	-45	-48	+0.03
G13	-1.55	-40	-45	-0.05	-2.14	-49	-54	+0.01
*13	-1.38	-38	-40	+0.01	-1.96	-46	-47	+0.02
G08	-1.09	-34	-38	+0.10	-1.66	-42	-44	-0.01
*08	-0.63	-28	-31	+0.02	-1.23	-37	-35	0.00
G11	-0.39	-25	-29	-0.06	-1.02	-34	-34	-0.03
*11	-0.15	-22	-26	+0.01	-0.80	-31	-29	0.00
G12	-0.15	-22	-30	-0.04	-0.82	-31	-34	+0.01
*12	+0.47	-14	-14	+0.05	-0.16	-22	-25	+0.01
G15	+1.08	- 6	- 8	+0.03	+0.49	-13	-16	-0.01
*15	+1.70	+ 3	- 3	+0.02	+1.12	- 5	- 9	+0.01
G14	+2.37	+11	+ 4	-0.04	+1.81	+ 4	+ 1	-0.01
*14	+3.33	+24	+18	-0.05	+2.78	+17	+11	0.00
G05	+4.61	+41	+42	-0.03	+4.08	+35	+35	+0.02

\+ Ice depth at GM estimated

Table 6.3 Transverse profile - ice depths from gravity anomalies

Bouguer correction for ice and the terrain correction. The volume of ice below the datum line (B) has not been corrected for and will lead to a negative gravity anomaly compared to the gravity expected at a horizontal rock plane. The anomaly will be proportional to $(\rho_{rock} - \rho_{ice})$.

In (ii) the volume above the datum line has been corrected for by the terrain correction and the Bouguer correction for ice. However, this still leaves volume C, with density $(\rho_{rock} - \rho_{ice})$, uncorrected. A positive anomaly will result.

From six rock samples randomly selected from the Vahsel moraine, the mean rock density was determined as 2.61×10^3 kg m^{-3} with a standard deviation of 0.15. As rock density in the vicinity of glaciers is difficult to obtain accurately from random moraine samples, the often quoted value of 2.67×10^3 kg m^{-3} was taken for ρ_{rock}. Hence the density anomaly $(\rho_{rock} - \rho_{ice})$ is 1.77×10^3 kg m^{-3}.

A first approximation to the ice depth was made by considering only a two dimensional glacier, and assuming the residual anomaly to be due to infinite Bouguer slabs of density $(\rho_{rock} - \rho_{ice})$. The ice depth at a station GM is non-zero and is unknown, but an ice thickness of 20 m at this point has been assumed from extrapolation of mean surface and bedrock slopes to the edge of the glacier. Evidence from moulins in this region supports a depth of about 20 m.

Because of the limited number of gravity stations, a numerical solution for the true depth was not attempted, and instead a graphical solution was sought. A simple graticule was constructed (Figure 6.5) in which the gravity effect in milligal of one compartment is given by

$$\Delta g = 2G (\rho_{rock} - \rho_{ice}) (r_{m+1} - r_m) (\cos\phi_{n+1} - \cos\phi_n)$$

where the length (m) of the inner and outer radii of the compartment are r_m and r_{m+1}, and their angles ϕ_n and ϕ_{n+1}. G is the universal gravitational constant $(= 6.67 \times 10^{-11}$ nt m^2 $kg^{-2})$. If $r_{m+1} - r_m$ is one centimetre, $\cos\phi_{n+1} - \cos\phi_n = 0.05$, and the scale of the diagram is 1:S, then the effect of each compartment is $6.67 \times 10^{-3} (\rho_{rock} - \rho_{ice})$S mgal (Griffiths and King, 1965).

Station	Observed Bouguer anomaly (mgal)	Ice depth from datum (assuming ∞ Bouguer slabs) (m)	Ice depth from datum Z (m)	Observed Bouguer anomaly - (Bouguer anomaly calculated for depth Z) (mgal)
G 43	+1.11	- 5	- 8	+0.05
G 11	-1.02	-34	-34	-0.03
G 10	-1.89	-45	-45	+0.01

Table 6.4 Longitudinal profile - ice depths from gravity anomalies.

A diagram of the glacier was constructed (using the depths estimated assuming infinite Bouguer slabs) to the scale 1:2000. The anomaly at any point P was then determined by laying the graticule on the datum line at P and counting the number of compartments (n) within the irregular glacier shape. Total anomaly at P is equal to n multiplied by the anomaly due to one compartment (= 0.024 mgal).

The calculated anomaly was compared with the observed anomaly and the ice depth corrected by:

$$(\text{ice depth})_{i+1} = (\text{ice depth})_i \frac{(\text{observed anomaly})}{(\text{calculated anomaly})}$$

and the process repeated until the calculated anomaly equalled the observed anomaly. A total of five iterations was required to obtain the final ice depths.

The final ice depths (Z) for the transverse and longitudinal profiles are shown in Tables 6.3 and 6.4. As the greatest error source in the observed anomalies is in the terrain correction, the ice depths for the uncorrected anomalies are also shown for the transverse profile.

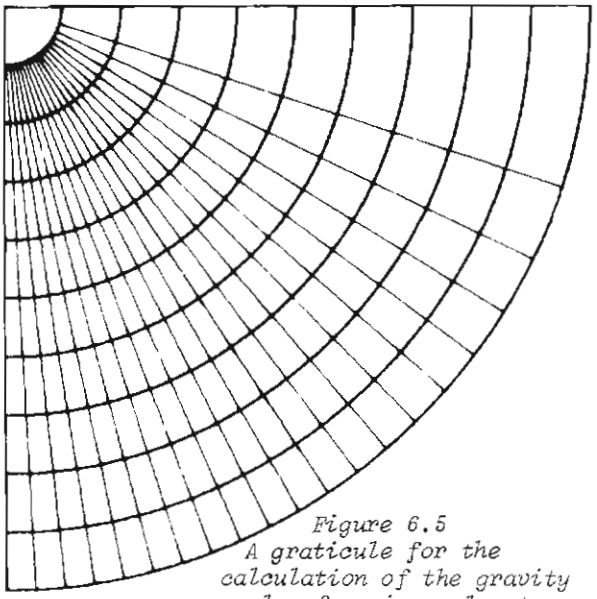

Figure 6.5 A graticule for the calculation of the gravity anomaly of an irregular two dimensional body.

All the above calculations have been made assuming a 2-D glacier. This is a reasonable assumption for the longitudinal line through G11, but not for the transverse line. At station G11 the effect of the longitudinal shape is to increase the ice determined for the 2-D case by three metres. However, with a similar longitudinal cross-section across the glacier, an equivalent depth increase will be needed at all the stations on the transverse line. As the depth at station GM has been arbitarily fixed at 20 m, no correction for a non two dimensional glacier has been made, but the expected error will be in the range 0 to +3 m.

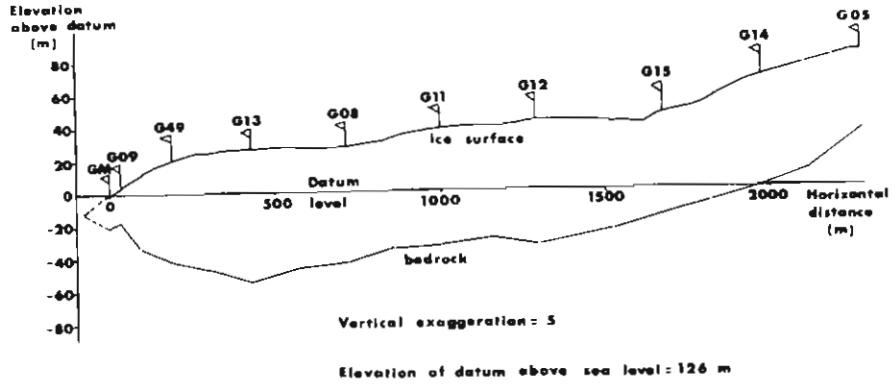

Figure 6.6 Transverse cross-section of the Vahsel glacier.

PRESSURE		CLOUD		PRECIPITATION		VISIBILITY		GLOBAL RADIATION	
DAILY	MEAN	DAILY	MEAN	DAILY	TOTAL	DAILY	MEAN	DAILY	MEAN
(mb)		(octas)		(mm)		(km)		MJm^{-2} Day^{-1}	MJm^{-2} Day^{-1}
± 3 mb				± 1				± 12%	
989.5		8		7.1		-			
989.8		8		8.6		6			
976.8		8		5.1		8		10.1	
986.5		7.5		0.3		18		9.9	
999.3	(988.4)	8	(7.9)	0.0	(21.1)	8	(10)	9.4	(9.8)
1008.0		8		0.8		4		12.0	
1000.8		8		0.8		0.5		7.6	
1004.9		7.8		0.0		6		28.2	
1012.1		8		0.5		5		15.4	
1011.6		7.5		8.4		13		17.0	
1006.8		8		1.0		4		10.7	
1000.0		7.5		0.8		13		23.2	
1007.0		7.5		<0.3		8		17.4	
1009.5		8		11.2		10		7.1	
992.4		7.7		2.5		4		17.1	
1002.5		8		0.3		5		21.1	
1012.9		8		2.5		1		3.9	
1005.4		8		2.3		2		17.1	
1003.0		7.3		<0.3		16		23.9	
1006.8		8		5.8		8		12.9	
999.8		8		8.6		4		6.0	
1005.3		6.7		5.1		13		27.4	
987.8		8		0.5		4		9.7	
993.4		7.7		4.1		10		17.2	
997.8		5.6		0.0		6		17.7	
1002.6		2.8		1.5		16		36.5	
1009.5		7.7		9.1		16		18.8	
994.8		7.3		9.4		2		16.6	
990.6		7.7		6.9		7		4.1	
998.3		7.3		<0.3		6		24.8	
1008.3		5.3		0.3		11		-	
1000.9		8		2.5		7		18.2	
987.9	1002.2	8	7.69	4.1	89.2	-	7	3.1	16.10
984.8		7.3		2.8		13		10.2	
989.1		8		1.0		5		4.9	
989.6		7.7		1.3		2		16.8	
999.0		8		0.3		6		4.3	
1004.3		8		16.5		-		19.2	(11.08)
995.4		7		<0.3		8		-	
1009.6		8		<0.3		5		-	
1018.3	(998.8)	8	(7.75)	<0.3	(22.1)	6	(6.4)	-	

meteorological data, 1971

curves for different latitudes in the northern and southern hemisphere from a number of different sources. A typical ablation scheme for the Vahsel glacier has been estimated from this data and is shown as the dotted line in Figure 8.1. The ablation rate at the firn line is then 3.1 m a^{-1}.

The accumulation distribution has been estimated from a precipitation of 3.1 m a^{-1} at 250 m above sea level, plus an increase with height of 0.5 m a^{-1} km^{-1}. Ahlmann (1948) found values of 0.4 and 0.5 m a^{-1} km^{-1} for similar island glaciers in high northern latitudes. The estimates of accumulation, ablation and balance are shown in Table 8.1.

The mass flux due to the area between any two elevations can be calculated from a knowledge of the above data together with elevation areas. Areas have been measured on the contour map of Figures 2.1 and 3.2 (from National Mapping map of Heard Island NMP/64/38 with the 200 m contour line corrected to fit the observed elevations). The calculated

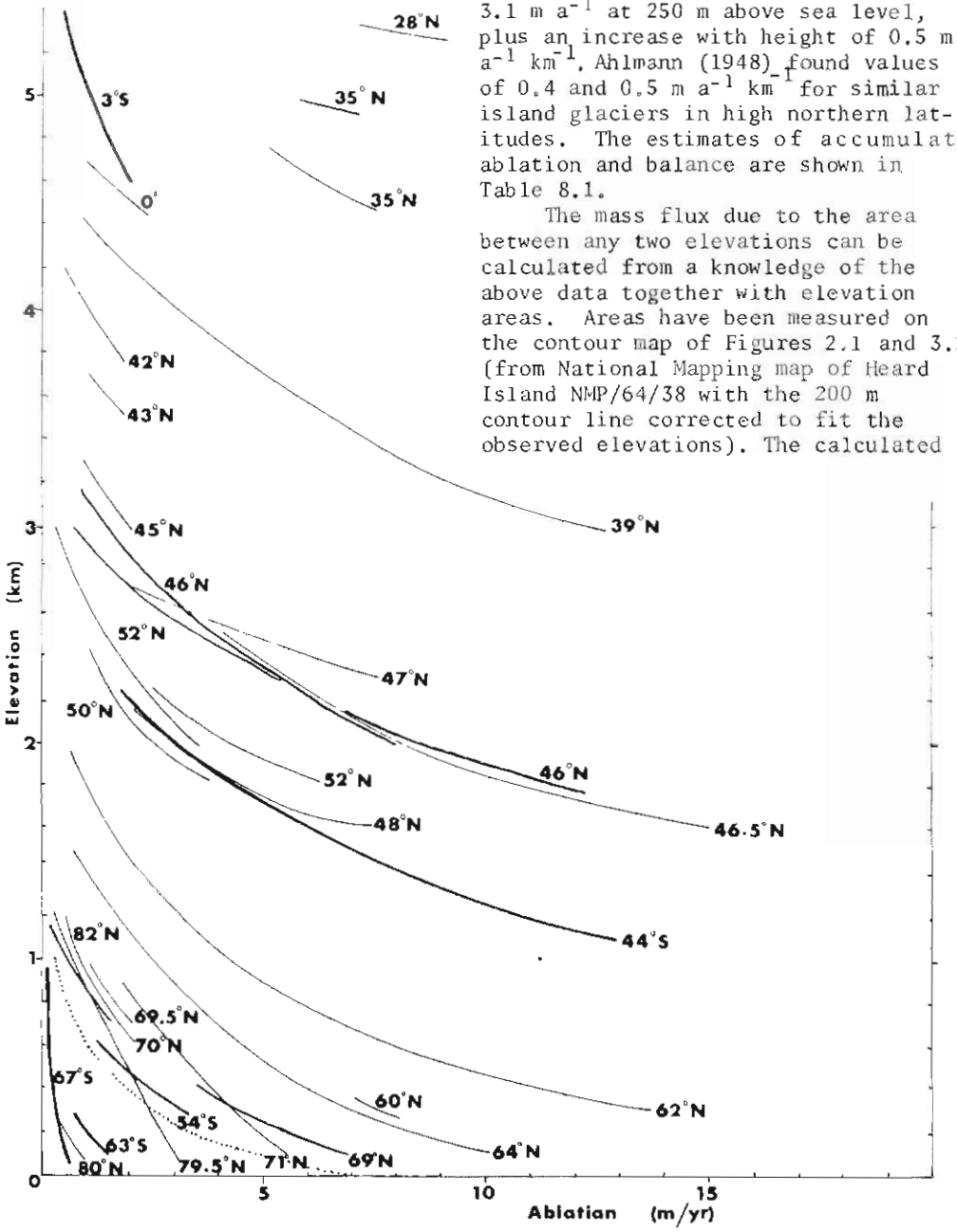

Figure 8.1 Ablation rate variation with elevation and latitude. (After Budd and Allison [1975]) (Vahsel Glacier estimate shown.....)

Elevation (m)	Precipitation (m a^{-1})	Ablation (m a^{-1})	Balance (m a^{-1})	Area (km^2)	Flux m^3 a^{-1} x 10^6	
0	2.9	-7.0	-4.1	3.9	-10.9	-15.3
100	3.0	-5.0	-1.5	5.9	- 4.4	
250	3.1	-3.1	0.0	3.6	+ 2.1	+18.0
400	3.2	-2.0	+1.2	2.2	+ 3.8	
600	3.3	-1.0	+2.3	2.0	+ 5.5	
1000	3.5	-0.3	+3.2	1.9	+ 6.6	
2400	4.2	-	+4.2			
Mean flux across firn line QF ~ 16.7 x 10^6 m^3 a^{-1}						

Table 8.1 Calculation of net balance and flux

fluxes are presented in Table 8.1. Mean flux across the firn line Q_F, is about 16.7 x 10^6 m^3 a^{-1}.

Now from Budd and Allison (1975),

$$Q_F = \bar{Y}\,\bar{V}\,Z = S_2\,Y\,S_3\,VZ = 16.7 \times 10^6$$

where $\bar{Y}$ and $\bar{V}$ are the mean cross-section width and velocity at the firn line and Z the maximum depth; S_2 and S_3 are shape factors such that

$$S_2 = \bar{Y}/Y \quad \text{and} \quad S_3 = \bar{V}/V$$

From Nye's (1965) results the value of S_3 can be obtained for different width to depth ratios. Assuming a shape factor S_2 = 0.7 and S_3 = 0.5 (since the glacier is very wide compared to its depth) and taking Y as three kilometres then

$$\Phi = VZ = 15.9 \times 10^3 \text{ m}^2 \text{ a}^{-1}$$

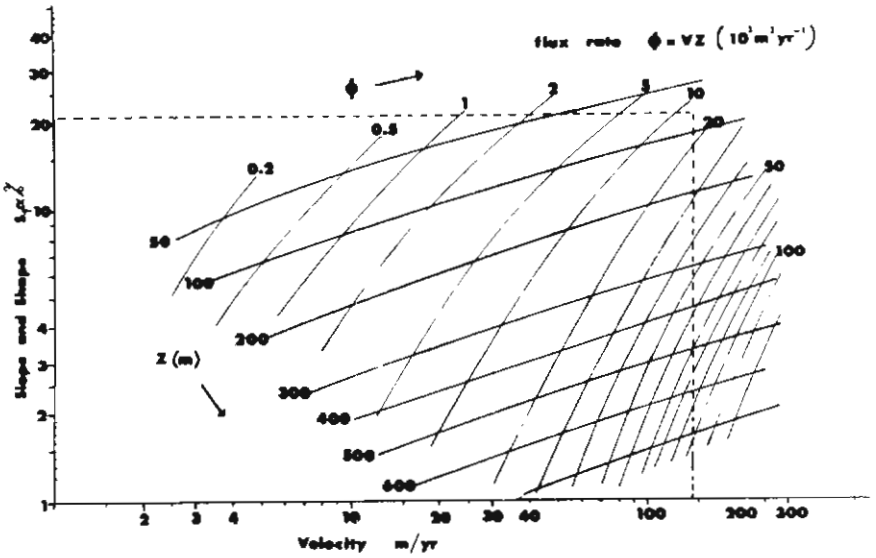

Figure 8.2 Ice thickness and flux variation with velocity and surface slope. (After Budd and Allison [1975])

Now using the empirical scheme of Budd and Allison (Figure 8.2) and taking the surface slope at the firn line, α, as 12^{o} or 21 per cent (estimated by extrapolating the surface in Figure 6.7 to 250 m) and the shape factor S_1 as 1, we read off a value of $Z \simeq 89$ m and $V \simeq 140$ m a^{-1}. These compare with the measured values at G11 of $Z = (72.5 \pm 15)$ m and $V = (117 \pm 38$ m $a^{-1})$.

Despite the large assumptions and simplifications made in calculating the mass balance of the glacier, the similarity between the observed and estimated velocity and depth indicate that the calculated mass balance of Table 8.1 is of the correct order.

8.2 Equilibrium State of the Vahsel glacier

The rate of surface lowering or increase at a stake moving with the glacier can be expressed as

$$\frac{\partial h}{\partial t} = A - V \tan \alpha - \frac{1}{\bar{Y}} \frac{\partial (\bar{Y}\ \bar{V}\ Z)}{\partial x} \qquad \text{(see section 5.1)}$$

which reduces to

$$\frac{\partial h}{\partial t} = A - V \tan \alpha + Z\ \dot{\bar{\varepsilon}}_z - \bar{V}\ \frac{\partial Z}{\partial x}$$

where $\dot{\varepsilon}_z$ is the vertical strain-rate $[\dot{\varepsilon}_z = -(\dot{\varepsilon}_x + \dot{\varepsilon}_y]$ and $\dot{\bar{\varepsilon}}_z$ is the mean value of $\dot{\varepsilon}_z$ over a vertical column of ice. $\bar{V}$ is the mean value of V over a vertical column of ice.

For the period 4 February 1971 to 28 February 1971 all the terms in the above equation can be evaluated from measurements made at G11.

At G11

		m a^{-1}	m a^{-1}
A	- 0.022 m/day ± 2%	-8.03 ± 2%	
$-V\tan\alpha$	$\tan \alpha = 0.24$ $V = (117 \pm 38)$ m a^{-1}	-2.81 ±32%	
$Z\dot{\bar{\varepsilon}}_z$	$Z = (72.5 \pm 15)$ m $\dot{\bar{\varepsilon}}_z \simeq 0.7\ \dot{\varepsilon}_z = 0.7\ (.038 \pm .004)\ a^{-1}$	+1.93 ±30%	
$-\bar{V}\ \frac{\partial \bar{z}}{\partial x}$	$\bar{V} = 0.7V = 0.7\ (117 \pm 38)$ m a^{-1} $\frac{\partial Z}{\partial x} = .027 \pm 10\%$	-2.21 ± 42%	
A	$- V \tan \alpha + Z\ \dot{\bar{\varepsilon}}_z - \bar{V}\ \frac{\partial Z}{\partial x}$		-11.12 ±23%
$\frac{\partial h}{\partial t}$	- 0.031 m/day ± 20%		-11.41 ±20%

The agreement between observed and calculated surface lowering is surprisingly good.

Now the surface lowering at any fixed point on the glacier is given by:

$$\frac{\partial Z}{\partial t} = A + Z\bar{\dot{\varepsilon}}_z - \bar{V}\frac{\partial Z}{\partial x}$$

and at G11 $\frac{\partial Z}{\partial t} = -8.3$ m a^{-1} ±20% for February. It should be noted that this is not the annual surface lowering rate but is the rate during the period of maximum ablation.

As stake G11 is close to the firn line, we can assume that the annual value of A is near zero and the mean annual surface lowering is given by:

$$\frac{\partial Z}{\partial t} = Z\bar{\dot{\varepsilon}}_z - \bar{V}\frac{\partial Z}{\partial x}$$

$$= (-0.28 \pm 1.51) \text{ m } a^{-1}$$

Unfortunately, the errors are too large to determine the equilibrium state of the glacier.

9. SUMMARY

9.1 Application to other Heard Island glaciers

Although measurements were only made on the Vahsel, this glacier is typical of those on Heard Island. All the Heard glaciers are characterized by steep surface slopes and a wedge like surface shape. The ablation zones are wider than the accumulation zones and the ratio of accumulation area to ablation ares is 1:1. This contrasts with the typical alpine glacier which nas a large accumulation basin feeding a tongue and an accumulation to ablation area ratio 3:1 (eg. Lliboutry 1965).

All the Heard glaciers can be expected to be fast flowing and shallow. Some, such as the Gotley, the main outflow glacier of the central dome, will be flowing considerably faster than the Vahsel and will be correspondingly thicker.

Because of the high velocity and quite short length (about 8 km) the particle residence time in the glaciers will be short. For the Vahsel Gl. the average residence time is of the order of 100 years. Hence time taken for the Heard glaciers to react to any balance changes will be correspondingly short.

9.2 Proposals for Future Work

Because of the large inaccuracies in the present study it can only be considered as a preliminary investigation of the Vahsel Glacier. It does, however, provide a valuable guide to the magnitude of parameters to be measured in any future intensive study.

With the prevailing poor visibility on Heard Island and the lack of good intersection stations around the Vahsel Glacier the survey measurements could be greatly improved by the use of electronic distance measuring equipment. Any future study should aim to extend the measurements to a number of transverse sections above and below the firn line and at least one longitudinal line down the glacier.

The difficulties in obtaining annual mass balance estimates from a study over a period of only one month is highlighted by this work. Any future investigation should endeavour to obtain annual net balance and velocity measurements for at least a number of representative stakes.

Gravity measurements probably provide the most convenient method of

obtaining ice thicknesses although a low frequency ice radar system would give better estimates. A number of ice thickness traverses should be run across and down the glacier.

Consideration should be given to establishing a temporary base camp close to the glacier to facilitate the measurements. Such a camp would also enable studies to be made on other suitable glaciers on Heard Island further from Atlas Cove.

ACKNOWLEDGEMENTS

The assistance of Terres Australes et Antarctiques Francaises in supporting the Heard Island expedition, and of all members of the Heard Island party, who gave freely of their time to help with the glaciology program, is gratefully acknowledged. In particular, Dr. R. Gendrin, leader of the party, provided active support of the program and the other members of the Australian contingent, Dr. G.M. Budd, and Messrs I. Dillon, I. Holmes and H. Thelander, spent many hours on the glacier.

Dr. W.F. Budd of the Antarctic Division gave active encouragement and assistance during the planning of the program and during the reduction and interpretation of the data.

REFERENCES

AHLMANN, H.W. (1948). *Glaciological research on the North Atlantic coasts.* R.G.S. Research Series: No. 1.

BUDD, G.M. (1964). Heard Island expedition 1963. *Polar Record* 12 (77):193.

BUDD, G.M. (1970). Heard Island reconnaissance 1969. *Polar Record* 15 (96): 335.

BUDD, G.M. and STEPHENSON, P.J. (1970). Recent glacier retreat on Heard Island. *Proceedings of the International Symposium on Antarctic Glaciological Exploration*, Hanover, 1968 (Edited Gow et al.). I.A.S.H. Publ. 86, pp. 449-58.

BUDD, W.F. and ALLISON, I. (1975). An empirical scheme for estimating the dynamics of unmeasured glaciers. *Snow and Ice Symposium.* (Proceedings of the Moscow Symposium, August 1971) : I.A.H.S. Publ. 104, pp. 246-256.

BULL, C and HARDY, J.R. (1956). The determination of the thickness of a glacier from measurements of the value of gravity. *Journal of Glaciology* 2(20): 755.

CORBATO, C.E. (1965). Thickness and basal configuration of the Lower Blue Glacier, Washington, determined by gravimetry. *Journal of Glaciology* 5(41): 637.

CROSSLEY, D.J. and CLARKE, G.K.C. (1970). Gravity measurements on "Fox" Glacier, Yukon Territory, Canada. *Journal of Glaciology* 9(57): 363.

GRIFFITHS, D.H. AND KING, R.F. (1965). *Applied geophysics for engineers and geologists.* Pergamon Press.

HAMMER, S. (1939). Terrain corrections for gravimeter stations. *Geophysics* 4(3): 184.

KANASEWICH, E.R. (1963). Gravity measurements on the Athabaska Glacier, Alberta, Canada. *Journal of Glaciology* 4(35): 617.

LAMBETH, A.J. (1950). Heard Island. Geography and glaciology. *Journal and Proceedings of the Royal Society of New South Wales* 84: 92.

LLIBOUTRY, L. (1965). *Traite de Glaciologie.* Masson, Paris.

MELLOR, M. (1964). Snow and Ice on the earth's surface. *Cold Regions Science and Engineering*, Part II, Section C. Cold Regions Research and Engineering Laboratory.

NYE, J.F. (1959). A method of determining the strain-rate tensor at the surface of a glacier. *Journal of Glaciology* 3(25): 409.

NYE, J.F. (1965). The flow of a glacier in a channel of rectangular, elliptic, or parabolic cross section. *Journal of Glaciology* 5(41): 661.

THIEL, E., LaCHAPELLE, E. and BEHRENDT, J. (1957). The thickness of Lemon Creek Glacier, Alaska, as determined by gravity measurement. *Transactions of A.G.U.* 38(5): 745.